Viscosity of rock mass at different structural levels

Chengzhi Qi [1,*]

Phone 86 10 68322492
Email qichengzhi@bucea.edu.cn

Chen Haoxiang [1]

Jiping Bai [2]

Jilin Qi [1]

Kairui Li [3]

[1] Beijing High Institution Research Center for Engineering Structures and New Materials, Beijing University of Civil Engineering and Architecture, Beijing, 100044 China

[2] Faculty of Computing, Engineering and Science, University of South Wales, Pontypridd, CF37 1DL UK

[3] School of Civil Engineering, PLA University of Science and Technology, Nanjing, 210007 China

Abstract

This paper examines viscosity of rock mass at different structural hierarchies. The study shows that viscosity and characteristic strain rate of rock mass vary at different structural levels. There exists one-to-one correspondence between characteristic scale level and strain rate. High viscosity with low characteristic strain rate occurs under macro-level, while meso- and micro-levels are characterized by low viscosity with high characteristic strain rate. Generally, with the increase in strain rate, deformation and fracture take place at decreasing scale levels, and

viscosity gradually decreases. With high characteristic strain rate at meso- and micro-levels, viscosity is inversely proportional to strain rate at these levels. Based on the analysis on viscosity at different structural levels, a unified description of viscosity is suggested and applied to the description of the strength–strain rate sensitivity of rock mass.

Keywords

Rock mass
Strain rate
Structural hierarchy
Viscosity

1. Introduction

Rock is a natural material that has complex internal structure with a wide spectrum of length scales. The complex internal structure of rock is expressed by a special term—structural hierarchy, which denotes the full spectrum of scale levels for structural elements of rock. Structural hierarchy of rocks may be regarded as the evolution result of "far from thermodynamic equilibrium" dynamical process in the earth system under the action of internal and external mechanical and physical factors in the forming process of rock and the following geological and geophysical process. Structural elements of rock mass are understood here as elements separated by cracks or weakened boundary surfaces between structural elements. Large structural elements contain smaller ones, and so on. The complex internal structure of rock mass makes it problematic for the representative volume element to be used in continuum mechanics. For rock mass, an important feature is the similarity of the internal structure in different sizes. In situ observations and sieving analysis in quarries [46] showed that a fundamental canonical series of the size l_i for geo-blocks exists.

$$l_i = (\sqrt{2})^{-i} l_0 \tag{1}$$

where $l_0 = 2.5 \times 10^6$ m is the radius of Earth's core; i is a positive integer. In situ observations [76] also showed that the worldwide pattern of fault formation may be represented in the form illustrated in Fig. 1, which

corresponds to the canonical series of geo-block sizes described in Eq. (1). The factor $\sqrt{2}$ may be understood with the help of the fault formation pattern shown in Fig. 1. Two mutually perpendicular fault systems form one mega-fault system. Two such mega-fault systems inclined to one another at an angle of 45° form a complete fault system. The geo-blocks of larger scale are separated by faults of larger width represented by ~~broader~~thicker lines in Fig. 1. The geo-blocks of larger scale are divided into two consecutively by the faults with smaller-scale size. It is interesting to point out that concrete mass is also cracked in the same way [77].

Fig. 1

Generalized fault formation pattern of different scale levels (after Tyapkin and Kiveliuk [76])

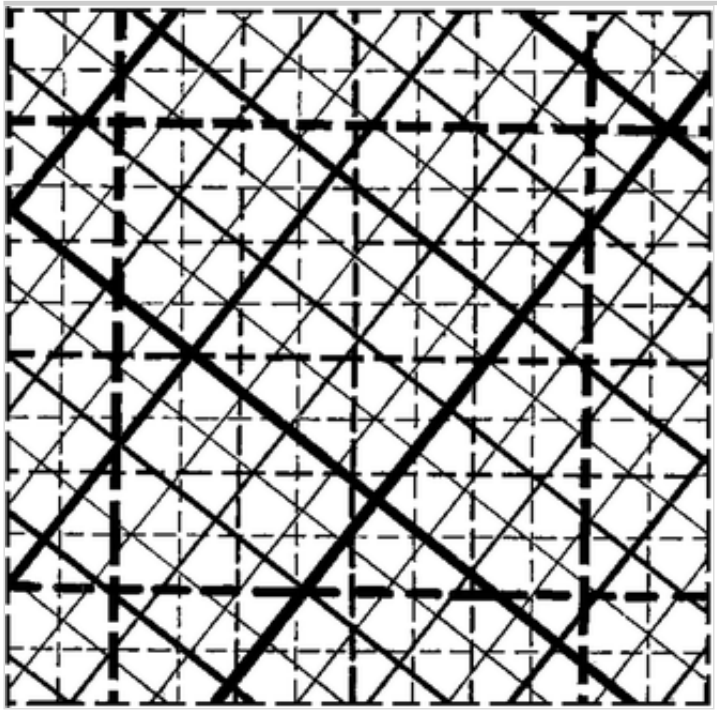

Housen and Holsapple [30] studied the fault and flaw size distribution. The 2D feature of faults and flaws is referred to as fault and flaw trace. Figure 2 shows the collected data for flaw trace lengths ranging from 100 μm to 10 km, a remarkable range of 8 decades [6, 27, 30, 42, 44, 51, 61, 67]. The shallow slope at the smallest sizes may be due to the difficulty to observe and count all of the smallest flaws at the particular resolution. For reproduction of the power-law behavior shown in Fig. 2, Housen and Holsapple used a “fully cracked” model, in which the average spacing

between faults and flaws is about equal to the flaw length. In this case, the number of flaws with a length larger than s in a sample with a volume of D^3 is.

$$n = (D/s)^3 \tag{2}$$

which is a special case of Eq. (1):

$$l_i = 2^{-i} \cdot l_0 \tag{3}$$

which describes one of the two mutually perpendicular fault systems shown in Fig. 1.

Fig. 2

Fault and flaw trace distributions for four types of rock (after Housen and Holsapple [30])

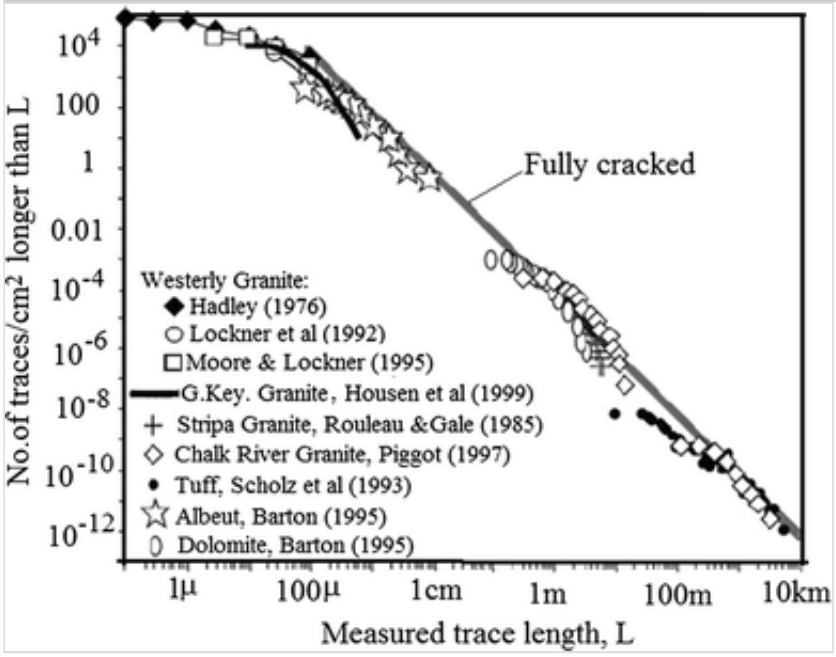

Equation (1) reflects the possible dense hierarchy. The hierarchical parameter, used in classical works of Sadovsky et al. [62], can be regarded as a special case of Eq. (1), i.e., $\left(\sqrt{2}\right)^3 = 2.83 \approx 3$, which may be considered acceptable due to the statistical nature of Eq. (1).

Shibi and Kamei [71], Qi et al. [56], Rahiman and Pettinga [58], Sherman [70] also studied the mechanism of general fault formation pattern. The study

by Kurlenia and Oparin [36] also showed that the atomic–ionic radii of different valent orbits of 98 elements in the table of Mendeleev obey canonical series as well. Therefore, canonical series Eq. (1) is valid for a scale size range significantly wider than 8 decades. Because of the complex internal structural hierarchy of rock mass, it is unnecessary to distinguish rock and rock mass.

AQ1

At every scale level, there are weak structural surfaces at which the deformation and fracture are greatly concentrated. According to in situ observations and laboratory experiments carried out by Kurlenia et al. [18], the ratio of the openings of cracks δ_i to the characteristic linear size of the blocks l_i separated by these cracks at the i-th scale level is stable and can be described by the following relationship which has a normal statistical distribution:

$$\mu_{\Delta}(\delta) = \frac{\delta_i}{l_i} = \Theta \cdot 10^{-2} \tag{4}$$

where Θ is a coefficient varying in the interval 1/2–2, and the parameter μ_{Δ} is termed as "geo-mechanical invariant" [37]. Equation (4) is valid even for the apparently "intact" materials like glass.

The "geo-mechanical invariant" of Eq. (4) is a statistical quantity based on the experimental and in situ observation data available to the authors of the concept. The ratio between the effective width and length of faults may not be linear and depends on the linear scale [17, 33, 66]. In this work, Eq. (4) simply indicates the proportionality between the effective width and length of faults for understanding the size effect of rock strength.

Internal structure of rocks has decisive impact on mechanical behaviors of rock mass under loading. For example, carbon and diamond have quite different mechanical behaviors because of the difference in their structures, although they are made of the same atoms. Generally, low strain rate processes take place at large-scale levels of geo-blocks. Accumulation of energy and deformation in the entire crust before occurrence of earthquakes at geotectonic level can serve as an example of such a case. As to the rupture

occurrence of earth crust in earthquakes, it is necessary to point out that such rupture is highly localized with high strain rate processes taking place in a narrow (small scale) band. The high strain rate processes are generally related to meso-structural or microstructural levels. A typical example is the process of deformation and fracture of material under intensive impact and shock loading. At levels between tectonic and meso–microscopical levels, intermediate strain rate processes take place, which are often encountered in engineering practice, for example, the fragmentation of rock caused by machines in mining industry.

Rock mass has many structural levels, but for practical application, such a structural hierarchy may be grouped into three levels: macro-, meso- and micro-levels. At present, there is no generally accepted definition for macroscale, mesoscale and microscale levels. Different authors give different definitions [3, 48, 72], but a tentative definition may be given as: The macroscale size from laboratory level to continental level spans from centimeters to thousands kilometers order; the mesoscale size may be in the order of grain size or their assembly; and the microscale size may be in the order of atom or dislocation size. However, the absence of a generally accepted definition of these three scale levels does not hinder our analysis.

The natural deformation of rock mass under external actions is the result of processes at microscopic scales, i.e., these processes have microscopic nature, but they are mainly concentrated at the weakened boundary surfaces between structural elements of rock mass. Strictly speaking, under external loads deformation proceeds at all scale levels. But under definite loading condition deformation mainly concentrates on weakened boundary surfaces of definite scale level. For example, under quasi-static loading condition (slow loading rate) deformation is mainly concentrated at the weakened boundary surfaces between larger structural elements of rock mass, and the localization of deformation results in separation of the body into macro-fragments at the final stage. Therefore, they may be attributed to the deformation process proceeding at macro-structural level, although the deformation at the weakened boundary surfaces has microscopic nature. Only at high loading rates when the microscopic structural elements are activated throughout the body uniformly can deformation and fracture be considered as processes at microscopic levels. Therefore, in the following, when we talk about

deformation and fracture proceeding at definite structural level we mean that deformation and fracture take place at the weakened boundary surfaces between structural elements at this structural level.

The accumulated data on viscosity make it possible to study the relationship between viscosity and structural levels of rock mass. Temporal deformation processes may be described as rheological change of mechanical properties and stress–strain state under loading. Traditionally, the change of stress–strain state is described with viscosity. In engineering practice, viscosity is considered as a constant of materials. In available literature, viscosity has large dispersion and often differs even in several orders. Obviously, this situation is related to the different scales at which deformation and fracture take place. At tectonic scale levels, deformation and relaxation proceed slowly, and viscosity η is within a range of $\eta = 10^{15} \sim 10^{23}$ even greater. But at meso- and micro-levels viscosity can be rather little. For example, under shock pressure when the meso-structural or micro-structural elements are activated, viscosity η is within a range of $\eta = 10^{1} \sim 10^{3}$.

Mathematically, viscosity η can be determined by the following equation [38]:

$$\eta = G \cdot \tau \tag{5}$$

where G is the shear modulus; τ is the relaxation time.

Equation (5) reflects such a nature of viscosity: The delay of deformation and fracture of media is due to the limited fracture propagation speed. This is confirmed by in situ observation and experimental data in a wide range of relaxation time [8] (see Fig. 3).

Fig. 3

Dependence of log (η/G) on log τ (after Belinsky et al. [8])

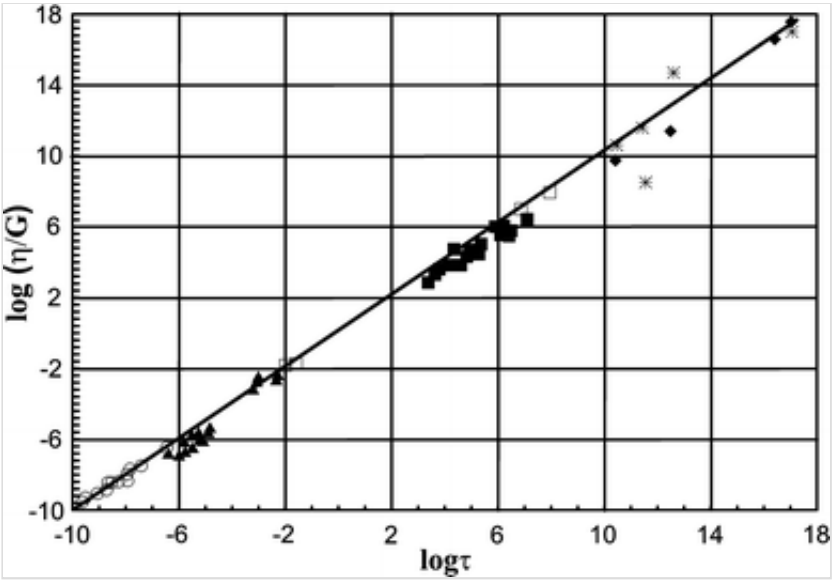

Behaviors of solid depend not only on properties of solid material, but also on loading conditions. Quasi-brittle material is only a conditional term to characterize the behaviors of rock mass under definite quasi-static uniaxial loading condition in laboratory, in which relaxation time τ is less than loading time t_{load}, i.e., when the Deborah number $De = \tau/t_{load} < 1$. When τ is much greater than t_{load}, i.e., when $De = \tau/t_{load} >> 1$, rock mass behaves as a rigid body. When τ is commeasurable with loading time t_{load}, i.e., when $De = \tau/t_{load} \sim 1$, rock behaves as a viscous material, for example, under long-term subcritical loading condition the earth's crust creeps (flows slowly). When τ is much less than t_{load}, i.e., when $De = \tau/t_{load} << 1$, rock behaves like a liquid; for example, under high loading rates rock mass behaves turbulently (flows rapidly).

In the study of deformation and fracture of rock mass, the authors of this paper found that viscosity decreases with strain rate. On the other hand, the characteristic strain rate at different scale levels of rock mass is inversely proportional to the scale levels of rock mass (see the following sections). Therefore, the viscosity magnitude might be proportional to the scale levels of rock mass. In order to confirm this conjecture, viscosity at different levels should be investigated. Can we give a unified physically sound description of viscosity at different scale levels? This question is originated not only from the intention to solve practical problems of rock mechanics, geophysics and engineering geology, but also from the curiosity to the natural law. Therefore, the solution of this problem is of both fundamental and practical meaning for

understanding the nature of deformation and fracture of rock mass. At present, viscosity has been studied at various scale levels separately, but no publications on a unified description of viscosity at different levels are available. The spectrum of length scales considered in this paper is wider than that considered in traditional geophysics. This is motivated by the intention to make the obtained law universal. It is necessary to point out that in this paper only quasi-brittle rock mass in earth's crust is studied, the mantle is not involved, i.e., effect of partially melting is beyond the scope of this investigation.

There are several factors that influence viscosity, including temperature, pressure and humidity. Investigations by Lawn and Wilshaw [39], Anderson and Grew [1], Atkinson [4], Atkinson and Meridith [5], Dove [15], Salganik et al. [65] showed that with the increase in temperature and humidity crack propagation speed increases, and viscosity decreases. Only when temperature approaches melting point may the strength of rocks decrease significantly. As the melting point of rocks is generally high enough, only at extremely high strain rates may temperature of rocks approach melting point. At continental or laboratory macroscale level, the range of temperature change is narrow in comparison with the scale change; the temperature effect may therefore be neglected. At microscale level, without extremely high strain rate, temperature does not approach to melting point, and the effect of temperature may also be neglected. Anderson and Grew [1], Atkinson [4] studied the influence of pressure on crack propagation and found that in some cases pressure promotes subcritical crack propagation, i.e., reduces viscosity; in other cases, pressure reduces subcritical crack propagation speed, i.e., enhances viscosity. At tectonic macroscopic level, the variation of magnitude and distribution of temperature, pressure and humidity is relatively small compared with the scale variation of rock mass. In laboratory, the variation of experimental temperature and humidity is also small, and applying high pressure is an approach to activate meso-scopic and microscopic levels, which is the object of this paper. Grain size and composition may also influence viscosity, but their variation is relatively small compared with the more than 10 order variation of length scale of rock mass. Therefore, in this paper the effect of temperature, pressure, humidity, grain size and composition of rock mass on

viscosity is the secondary consideration, and this study will mainly focus on the scale levels of rock mass.

Based on the above analysis, this paper is intended to examine the viscosity at different structural levels and attempt to unify viscosity at different scale levels. Firstly, the relaxation model of Maxwell type for rock mass will be used to obtain the relationship between sample size and characteristic strain rate so as to establish the one-to-one correspondence between sample size and characteristic strain rate. Secondly, the viscosity at macro-scale, micro-scale and meso-scale levels will be examined, respectively, indicating the decrease in viscosity with the decrease in scale from tectonic macro-scale level to micro-level and correspondingly with the increase in strain rates. Thirdly, based on the analysis of viscosity at different structural levels, a unified description of viscosity at different levels will be suggested. Finally, the proposed unified description of viscosity will be applied to the description of the strength–strain rate sensitivity of rocks, so as to verify the validity of the model.

2. The one-to-one correspondence between characteristic scale level and strain rate

Experimental and theoretical investigations [57] with in situ observations [69] revealed that deformation and fracture of rock-like materials are governed by the laws of Maxwell bodies. The internal structure has a decisive impact on mechanical behaviors of rocks. If the strength of crystals with ideal regular lattices is their theoretical strength, the strength of real materials is about 2–3 orders lower than the theoretical strength of ideal crystals. This is obviously a result of the stress concentration and strain localization from the complex hierarchic internal structure of real materials.

As a reference medium, a crystal with ideal regular lattices will be considered. When such ideal crystal is subjected to loading which is high enough but well below the strength limit, the damage, fracture and stress relaxation will not occur in the crystal. However, if the ideal crystal is replaced by real rock mass with complex internal structure, stress concentration and successive damage and fracture may occur. Consequently, part of the stresses in rock mass will relax. Therefore, the stresses in such

solid can be divided into two components: elastic stresses caused by the reversible volume and shear deformations, and the local inelastic stresses due to structural heterogeneities which are responsible for the irreversible deformations. As to the residual stresses (inelastic stresses), they arise at definite strain rate, and relax with time. The evolution of the residual stresses may be described by Maxwell model as proposed in [57], which here is generalized to arbitrary stress states. The evolution equation for the residual deviatoric stresses Δs_{ij}^{l} due to structural heterogeneities or internal structure may be described by Maxwell model.

$$\frac{\mathrm{d}\Delta s_{ij}^{l}}{\mathrm{d}t} = 2\rho c_s^2 \dot{e}_{ij} - v\frac{\Delta s_{ij}^{l}}{l} \tag{6}$$

where Δs_{ij}^{l} are the residual stress deviator components in structural heterogeneities with the characteristic scale l; e_{ij} are the deviatoric strain rate components; ρ is the density of the medium; v is the relaxation speed, which may be considered as the effective crack propagation speed; c_s is the propagation speed of the elastic shear wave. Here, it is supposed that all residual stress components relax with the same relaxation time. Essentially, $l/v.v$ may be considered as relaxation time $\tau = l/v.v$. The first term on the right-hand side of Eq. (6) describes the elastic loading, while the second term denotes stress relaxation due to cracking.

The main feature of this model is that the relaxation rate of the residual stresses in heterogeneities is proportional to the magnitude of the residual stresses and inversely proportional to the dimension of the heterogeneities. It is necessary to note that this model is applicable not only to different rock-like materials with great range of relaxation time, but also to highly viscous fluids for which the relaxation time is relatively short [38].

For constant strain rate, the solution of Eq. (4) has the following form:

$$\Delta s_{ij}^{l} = 2\rho c_s^2 \dot{e}_{ij}\frac{l}{v}\left[1 - e^{-vt/l}\right] = 2\rho c_s^2 \dot{e}_{ij}\tau\left[1 - e^{-t/\tau}\right] \tag{7}$$

For a short loading time $t << \tau$, there is no enough time for the relaxation process to develop, Eq. (7) gives $\Delta s_{ij}^{l} \approx 2\rho c_s^2 \dot{e}_{ij} t = 2\rho c_s^2 e_{ij}$, i.e., the residual

stresses will increase linearly with time, and the final amplitude of stresses is limited by the duration of loading process.

For a long loading time $t >> \tau$, loading process is limited by the relaxation time. In this case, Eq. (7) yields

$$\Delta s_{ij}^{l} \approx 2\rho c_s^2 \dot{e}_{ij} \frac{l}{v} \tag{8}$$

For the occurrence of macro-fracture, it is necessary that the loading time is greater than relaxation time $t > \tau$. Therefore, Eq. (8) is reasonable to reflect macro-fracture in the rock samples.

Substituting Eq. (8) into the expression for intensity of residual stress deviator $\Delta\sigma_I = \sqrt{3\Delta s_{ij}^{l} \Delta s_{ij}^{l}/2}$, it gives

$$\Delta\sigma_I = 3\rho c_s^2 \dot{\varepsilon}_I \frac{l}{v} \tag{9}$$

where $\dot{\varepsilon}_I = \sqrt{2\dot{e}_{ij}\dot{e}_{ij}/3}$ is the strain rate intensity.

It can be seen from Eqs. (8) and (9) that if the applied strain rate is fixed, the larger the size of the heterogeneous elements is, the greater are the residual stresses. If the size of the body is infinite, it is always possible to find sufficiently large structural heterogeneous elements so that the residual stresses are high enough to cause the fracture of the body. In this way, at constant strain rate a parameter with length dimension is introduced in the model. Stress concentration causing residual stress in heterogeneous media is the main cause for material fracture. When the intensity of residual stresses $\Delta\sigma_I$ reaches the strength σ^* at this scale level fractures take place. In this case, Eq. (9) may be rewritten as

$$\sigma^* = 3\rho c_s^2 \dot{\varepsilon}_I \frac{l}{v} \tag{10}$$

Equation (10) indicates that the dynamic strength of rock-like materials is proportional to the sample size at the same strain rate. This has been

confirmed by the experiments carried out by Hong et al. [28], who have performed series of refined experiments on size effect of rock dynamic strength and strain rate sensitivity by using split Hopkinson bar at room temperature. One of their experimental results on dependence of dynamic strength against sample diameter of granite is illustrated in Fig. 4. It is found from Fig. 4 that the dynamic strength of granite samples is proportional to sample size. This law is also valid for concrete structure: the larger the structure is, the stronger is the strain rate effect [47]. The increase in dynamic strength of rock samples with the increase in sample size is named as dynamic size effect, which is opposite to static size effect (decrease in strength of rock samples with the increase in sample size). The implied physical mechanism of dynamic size effect and its relation with static size effect have been explained in [55]. The essence of the dynamic size effect is that because of the finiteness of crack propagation speed, when the strain rate is well above certain characteristic strain rate, dynamic loading process takes predominant role in comparison with relaxation process. The stresses in sample have no enough time to relax completely. The larger the sample size is, the more time is required for cracks to propagate through the sample, and the higher the applied stresses are before the complete fractures of samples occur.

Fig. 4

Size effect of rock strength under different strain rates (after Hong, Li et al. [31])

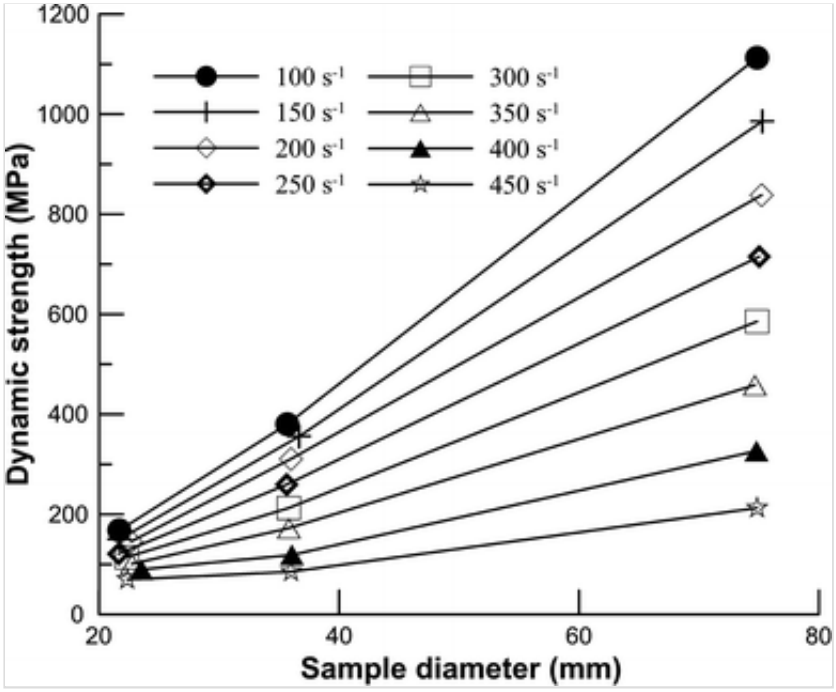

The length scale l in Eq. (10) should be understood from the viewpoint of internal structural hierarchy. For sample with size L, the maximum possible structural element size of the sample is $l = L$. According to Eq. (10), the characteristic strain rate necessary for the fracture of the sample is $\dot{\varepsilon}_L = \sigma^* v / \left(3\rho c_s^2 L\right)$. If the applied strain rate $\dot{\varepsilon}$ is greater than $\dot{\varepsilon}_L$: $\dot{\varepsilon} > \dot{\varepsilon}_L$, the fracture process will select one characteristic size l_f for the fragmentation of the sample according to Eq. (10), as

$$l_f = \frac{\sigma^*(\dot{\varepsilon})}{3\rho c_s^2} \cdot \frac{v}{\dot{\varepsilon}} \tag{11}$$

which is the minimum size of the heterogeneity at which concentrated stress equals to the strength at a given strain rate [57].

For plastically non-compressible rock, the Poisson's ratio is $\mu \approx 0.5$, and Young's elastic modulus is $E = 2(1 + \mu)G \approx 2(1 + 0.5)\rho {c_s}^2 = 3\rho {c_s}^2$. Therefore, the term $\sigma^* / \left(3\rho c_s^2\right)$ on the right-hand side of Eq. (11) represents the magnitude ε^* of deformation at strength limit σ^*, and Eq. (11) may be rewritten as

$$l_f = \varepsilon^* \cdot \frac{v}{\dot{\varepsilon}} \tag{12}$$

Therefore, the level at which deformation and fracture proceed is not the scale level L of the sample, but the scale level of l_f according to Eq. (11). In the following sections, when we talk about the scale level of deformation and fracture, we mean the activated scale level of internal elements according to Eq. (11).

It is clear from Eq. (11) that with the increase in strain rate meso-scopic and microscopic scale levels of internal elements will be involved in deformation and fracture process successively.

For many rock-like materials in a large range of strain rates, a lot of experiments have shown that the relationship between the dynamic strength and the strain rate has the following form [12]

$$\sigma^* \propto (\dot{\varepsilon})^{1/3} \tag{13}$$

Substituting Eq. (13) into Eq. (11), it becomes

$$l_f \propto (\dot{\varepsilon})^{-2/3} \tag{14}$$

Kipp and Grady [31] obtained the following relationship by using the model of Mott fracture with dissipation

$$l_f = \left(24W/\rho\dot{\varepsilon}^2\right)^{1/3} \tag{15}$$

where W is work of fracture; ρ is the density of medium. This result agrees with that from Eq. (14).

The above-mentioned experimental data and theoretical results confirm the validity of presented model with internal structure.

Equation (11) shows the one-to-one correspondence between characteristic scale level and characteristic strain rate. Propagation speed v of crack depends on loading conditions. Experimental observations of fracture propagation by Bieniawski [9], Lawn and Wilshaw [39], Anderson and Grew [1], Atkinson [4], Atkinson and Meridith [5], Dove [15], Salganik et al.

[65] indicate that crack may grow for energy lower than the critical limit of fracture. The experimental curve is shown in Fig. 5. At micro-scale, the tensile failure due to the subcritical propagation of cracks may represent the main micro-mechanism of creep at the macro-scale. In regime I, the rate of thermally activated stress corrosion reaction controls the speed of crack growth. Regime II is mainly determined by the rate of transport of reactive species to crack tips. In regime III, the speed of crack growth increases drastically up to failure and is relatively independent on the chemical environment and is controlled by mechanical rupture [21, 50]. This typical three-mode regime is characteristics of rocks, ceramics and glasses.

Fig. 5

Dependence of crack propagation speed v on stress intensity factor K (after Lawn et al. [1, 4, 5, 15, 21, 27, 65])

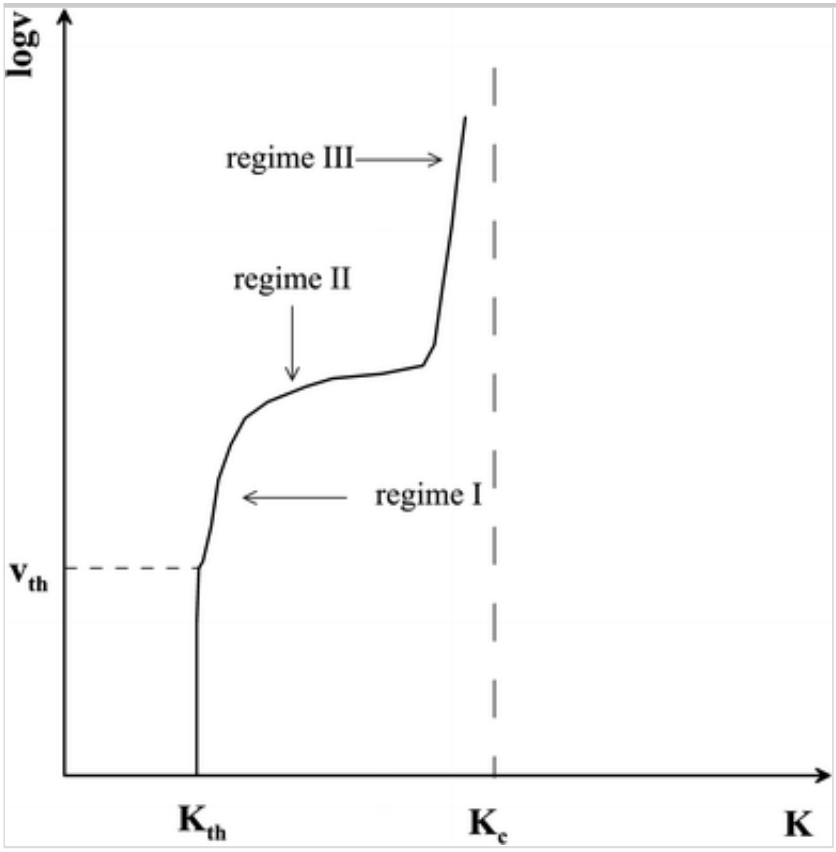

From Fig. 5, it is also clear there exists a threshold of stress intensity factor K_{th}, below which the crack propagation speed will have a drop from v_{th} to zero, and the material will "never" fracture from a mechanical viewpoint. The corresponding strain rate $\dot{\varepsilon}_{th}$ may be determined according to

$\dot{\varepsilon}_L = \sigma^* v_{\text{th}} / \left(3\rho c_s^2 L\right)$ for definite L and v_{th}. Generally, v_{th} ranges from 10^{-6} to 10^{-11} m/s dependent on material properties and environmental conditions. Experiments on lifetime of macro-samples do show that when the applied load is less than the threshold σ_∞, the lifetime of macro-samples τ_{life} will increase dramatically, as shown in Fig. 6, and materials will "never" fracture [49]. This explains the one-to-one correspondence between characteristic scale level and characteristic strain rate.

Fig. 6

Dependence of lifetime τ_{life} of materials on applied loads σ (after Petrov [49])

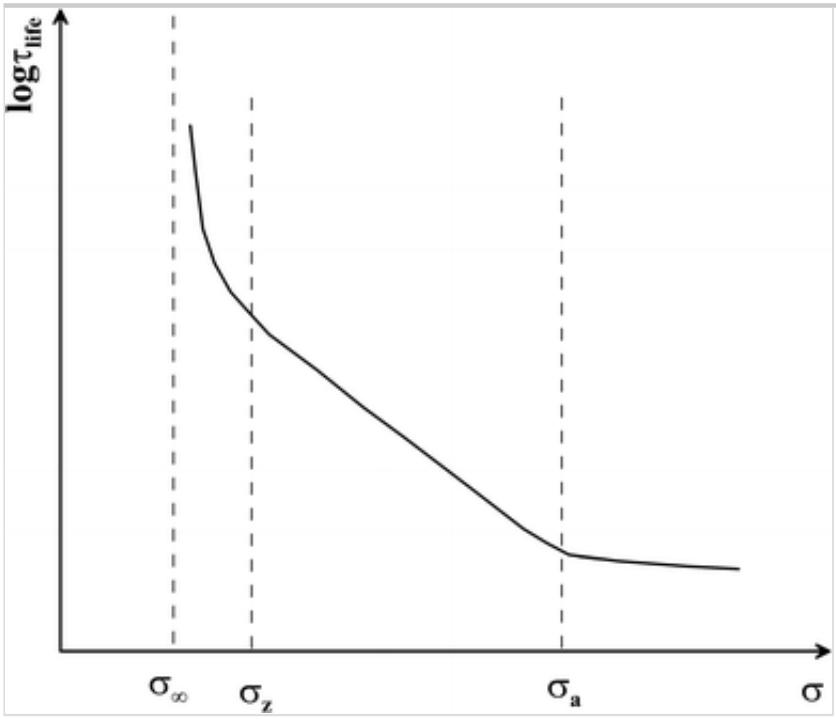

For system of earth's crust materials "never" fracturing does not mean that the viscosity will be arbitrarily high, because the "living" system of earth's crust is in non-equilibrium stressing state. The giant continental plates of earth's crust are drifting at definite velocity, seismic events of different intensities are proceeding regularly, and the relaxation times at different levels are not infinite. Therefore, viscosity cannot be arbitrarily high.

Experiments and theoretical investigations showed the finiteness of maximum crack growth speed (generally less than the Rayleigh wave speed C_R) [11, 13, 16, 18–20, 22, 45, 59, 75, 78, 79]. Figure 7 shows the dependence of crack propagation speed on applied stresses [20]. As shown in Fig. 5 and 7,

the dependence of crack growth speed on stress intensity factor and stress is nonlinear.

Fig. 7

Dependence of crack propagation speed on applied stress (after Finkel [20])

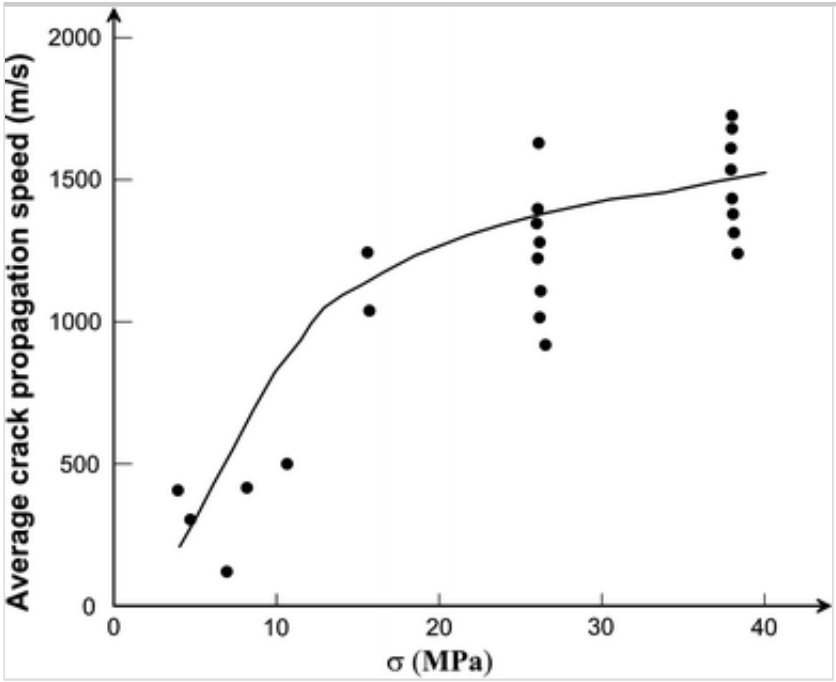

For mode II cracks, the maximum crack growth speed is also limited. Even for the interfacial super-shear crack propagation, the maximum crack growth speed is also limited by the longitudinal wave speed [60]. At high strain rates, when the crack growth speed exceeds definite value, branching will occur; in this case, the growth of crack will be retarded. At high strain rates, the failure mode may be mixed, but the resulting effective crack propagation speed is limited. Hence, the developed model is applicable here.

Therefore, there are two characteristic crack propagation velocities: the crack growth speed v_{th} corresponding to K_{th} and effective dynamic crack growth speed limit v_c.

With the help of Eq. (11), it is easy to understand why the giant continental plates only exist under slow strain rate condition, and for pulverization of materials the high strain rate is necessary.

3. The viscosity at macro-level

In this section, we will show that at tectonic macro-level viscosity is very high, and it decreases with the decrease in scale level of geo-blocks.

At tectonic macro-level, accumulation and release of deformation energy proceed in the form of earthquakes. Some seismological observations [43] have shown that after occurrence of earthquakes with magnitudes $M \geq 7$, eighty-four days are needed for rock mass to restore its initial seismological condition, even several years in some cases. Hence, relaxation time τ may change from $\tau_1 = 84$ days $\approx 7 \times 10^6$ s to $\tau_2 = 10$ years $\approx 3.1 \times 10^8$ s. Taking G ≈ 40–45 GPa (for Baikal rift zone), the viscosity $\eta \approx 10^{17} \sim 10^{19}$ Pa·s [43]. The estimation of the effective viscosity from experimental data strongly depends on the timescale of the data set as shown in [34], and the evaluation of viscosity based on seismological observations may be somewhat rough. Here, it is only to show that viscosity at tectonic macro-level is really very high.

Viscosity is directly related to structural levels. Comparing available values of viscosity η with the density of the active faults of the Cenozoic era within the trapezoid area 5 × 5° on the earth surface and making an assessment, it is not difficult to notice the inverse proportionality between them (see Fig. 8a [43]).

Fig. 8

a Relationship between viscosity and fault density **b** gradient of vertical movement speed (after Lysak and Levi [43])

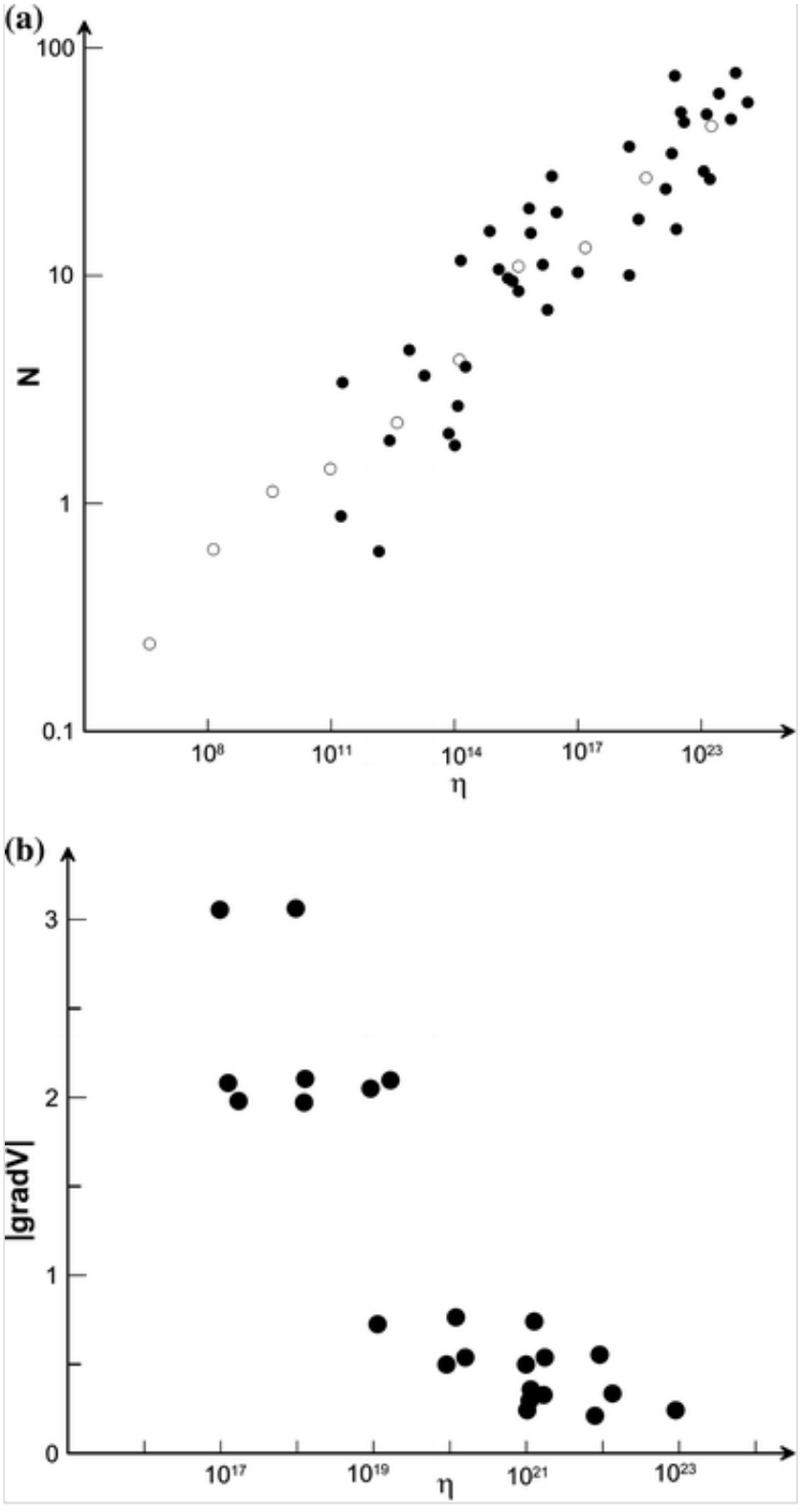

Statistics reveals that the correlation between the fault density in an 1 km^2 area n and fault size L can be expressed as [69]

$$L = \frac{c}{n^{\beta}};\ n = \frac{d}{L^{\alpha}} \tag{16}$$

where c, d, α and β are constants.

Based on Eq. (16), it can be concluded that viscosity of rock mass decreases with the decrease in its size.

Equation (16) also shows that in the process of the formation of a fault net, i.e., in mega- and macro-fracture of rock mass under natural conditions, some common fracture laws appear without dependence on tectonic activation intensity and tectonic evolution history. Comparison between the data obtained in geological investigations and the experimental data for Maxwell bodies indicates that the characteristics of the behaviors of Maxwell bodies in fracture are identical to that of the formation of the faults with different lengths in regions with different tectonic evolution history and different activation intensity. Hence, it can be concluded that in the process of the fault net formation, the earth's crust behaves as a Maxwell body, i.e., as a elastoviscous body.

Figure 8b shows that viscosity is inversely proportional to the gradient of the speed V of vertical neo-tectonic movement $|gradV|$, which is considered as an indicator of deformation rate of the media [43].

The density N of faults in the lithosphere is closely related to the gradient of the speed V of vertical neo-tectonic movement $|gradV|$. This relationship is demonstrated in Fig. 9, which clearly shows that regions with higher fault density have higher $|gradV|$ and lower viscosity [43]. Figures 8 and 9 show the mutual dependence of viscosity η, the scale sizes of rock mass $1/N$ and the strain rate $\partial \gamma_{xz}/\partial t$.

Fig. 9

Relationship between fault density and gradient of vertical movement speed (after Lysak and Levi [43])

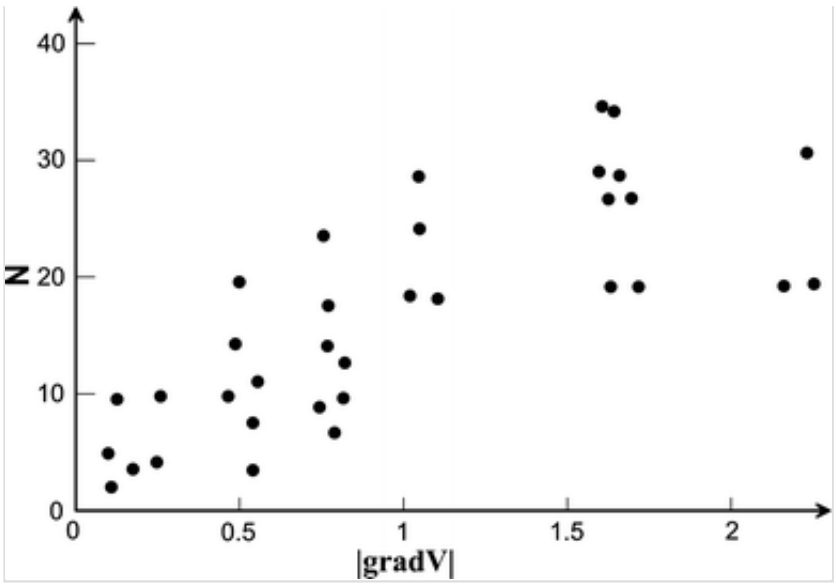

The quantity $|gradV|$ is in fact the shear deformation rate of rock mass. This can be seen from the following derivation.

Let the non-zero displacement component in the direction of vertical coordinate z be w, the other two displacement components u and v in the directions of two horizontal coordinates x and y are $u = 0$, $v = 0$; then, shear deformation rate may be expressed by the gradient of w in the direction of x

$$\left|\frac{\partial \gamma_{xz}}{\partial t}\right| = \left|\frac{\partial}{\partial t}\left(\frac{\partial w}{\partial x} + \frac{\partial u}{\partial z}\right)\right| = \left|\frac{\partial}{\partial t}\left(\frac{\partial w}{\partial x} + \frac{\partial 0}{\partial z}\right)\right| = \left|\frac{\partial}{\partial t}\left(\frac{\partial w}{\partial x}\right)\right| = |gradV| \quad 17$$

Therefore, viscosity of rock mass decreases with the increase in the deformation rate.

The data in Fig. 8b may be approximately represented by a straight line

$$\ln \eta = b - \alpha |gradV| = b - \alpha \left|\frac{\partial \gamma_{xz}}{\partial t}\right| = b - \alpha |\dot{\gamma}_{xz}| \quad 18$$

then

$$\eta = e^{-b} \exp(-\alpha |\dot{\gamma}_{xz}|) = \frac{\eta'}{\exp(\alpha |\dot{\gamma}_{xz}|)} \approx \frac{\eta'}{1 + \chi |\dot{\gamma}_{xz}|} \quad 19$$

where b, χ and η' are constants.

From Fig. 9 together with Eq. (16), the relationship between the structural levels and the deformation rate can be obtained as follows:

$$\dot{\gamma} = \left(\frac{d}{L^{\alpha}}\right)^{m}, (m \leq 1) \quad \text{and} \quad L = \left[\frac{d}{\dot{\gamma}^{1/m}}\right]^{\frac{1}{\alpha}} \tag{20}$$

At macro-scale level in the orders of cm and mm, viscosity η of materials is experimentally determined by the shock loading method. The upper limit of η is 10^5 to 10^6 Pa s, and the lower limit of η is determined by the following Eq. [3]

$$\eta \approx \rho_0 u \lambda D t \tag{21}$$

where ρ_0 is the initial density of materials; D is the shock wave speed; u is the particle speed; λ is the coefficient in the compression law of $D(u)$; the width of shock wave is measured by time t. For example, shock experiments of NaCl at room temperature shows that the viscosity η changes in the diapason of $10^3 \sim 10^4$ Pa s [7].

In summary, we can see that viscosity at tectonic macro-level is very high and gradually decreases with the decrease in activated structural element size of rock mass. At laboratory macro-scale level, viscosity is more than ten orders less than that at tectonic macro-level.

4. The viscosity at meso-level

The meso-level bridges macro- and micro-levels. The behaviors of materials at meso-level affect that of materials at macro-level. The process of deformation and fracture of rock mass and energy transition between macro- and meso-levels are accompanied by the formation of new structures. Rock mass has multi-level structures. The strength at the boundary surface in rock is lower than that of grains. Under intensive shock loading, rock mass and other solids behave hydrodynamically at mesoscale level [24, 25, 29, 41]. Mechanically, the turbulence nature of the motion of media is explained by the fact that the applied external loading is significantly greater than the shear strength of media, and the loss of shear stability leads to the formation of

shear zones, the local relaxation of elastic stresses and the appearance of rotational motion mode of media. The pulsation and dispersion of meso-particle velocity strengthen the turbulent of motion of media. Physically, the turbulence nature of the motion of media under strong shock loading may be interpreted as a highly excited state [48], which is characterized by the maximum non-equilibrium thermodynamical potential and should be considered as the initial state. In this case, the distribution function of atoms in space is substantially different from that for ideal crystals. In addition to structural states of initial crystals under highly excited state in interstitial spaces, new allowable structural states emerge. These new structural states may be vacant states or states taken by the highly excited atoms. In crystals, new degrees of freedom emerge. Highly excited crystals, in essence, become superposition of several structures, and the number of allowable structural states in this system is significantly greater than that of atoms. These states in crystals are called highly excited states or atom–vacancy states. The main point of this approach lies in that any local breakage of structure of highly excited crystals should be considered not simply as defect, but as a new allowable structural state genetically laid in an electron energy spectrum of crystals. Predicting all possible structural states of a solid can be realized only in the framework of theory of highly excited states of crystals, in which the number of degrees of freedom in a system is more than that in crystals under ground state. The consequence of the turbulent motion of media is the power-law fragment size distribution [24, 25]. A statistical approach based on the random particle walk reproduced the power-law fragment size distribution [73]. Hence, it would be rational to use statistical physics to describe the interaction between rock particles.

By assuming that $\vec{R}_i$ is the position of *i*-th particle at moment *t,* the dynamics of particles can be described by the time-dependent distribution function $\psi\left(\vec{R}_1, \vec{R}_2, \ldots, \vec{R}_N\right)$. Then, the probability ψ for finding a particle at a given point and time is determined by the following Eq. [10]

$$\frac{\partial \psi}{\partial t} = -\sum_N \frac{\partial}{\partial \vec{R}_i}\left(\vec{R}_i \psi\right) \tag{22}$$

Equation (22) may be transformed into equation [14]

$$\frac{\partial \psi}{\partial t} = -\frac{\partial}{\partial \vec{R}}\left(D\frac{\partial}{\partial \vec{R}} - \vec{v}\psi\right) \tag{23}$$

where $\vec{v}$ is the relative speed of particles; D is a diffusion coefficient; and $D = kT/\varsigma$, where $\varsigma = 2\pi a\eta$, with a being the particle radius.

Then, the local configuration average stress created by a given flow field $\vec{v}$ is determined by the following formula

$$\bar{\sigma}_{\alpha\beta}(\vec{r}) = \int \bar{\sigma}_{\alpha\beta}\left(\vec{r}, \vec{R}\right) \cdot \psi\left(\vec{R}\right) d\vec{R} \tag{24}$$

The spatial average stress over the volume V containing N particles gives the spatial independent stress components:

$$\left\langle \bar{\sigma}_{\alpha\beta}(\vec{r}) \right\rangle = \frac{1}{V}\int \bar{\sigma}_{\alpha\beta}(\vec{r}) d\vec{r} = \frac{1}{V}\left[\int_{V_2} \bar{\sigma}_{\alpha\beta}(\vec{r})\, d\vec{r} + \sum_{N}\int_{V_1} \bar{\sigma}_{\alpha\beta}(\vec{r})\, d\vec{r}\right] \tag{25}$$

where V_1 is the volume occupied by particles, and V_2 is the volume of media between particles.

The effective viscosity is determined by

$$\eta_{ij} = \langle \sigma_{ij} \rangle / 2\left\langle \dot{e}_{ij}^{0} \right\rangle \tag{26}$$

where $\left\langle \dot{e}_{ij}^{0} \right\rangle = \frac{1}{V}\int_{V} \dot{e}_{\alpha\beta}(\vec{r})\, d\vec{r}$ is the macroscopic average strain rate.

Also,

$$\eta = \eta_2(1-\phi) + \frac{\phi\langle \sigma_{\alpha\beta} \rangle_1}{2\dot{e}_{\alpha\beta}^{0}},\ \alpha \neq \beta \tag{27}$$

where $\eta = \eta_{\alpha\beta}$, $\eta_2 = \alpha\eta(\varphi)$, α is a constant, φ is the volume fraction of particles, and

$$\langle \sigma_{\alpha\beta} \rangle_1 = \frac{1}{V_1}\int_{V_1} \bar{\sigma}_{\alpha\beta}(\vec{r})\, d\vec{r} \tag{28}$$

In two-dimensional cases, the center of the spherical particle is considered as the origin of spatial coordinates, where the speed field is given by

$$\vec{v} = \dot{\gamma} \cdot z\vec{j} \tag{29}$$

Substituting Eq. (29) into Eq. (23), with consideration of Eq. (24), yields

$$D\frac{d^2\bar{\sigma}_{yz}}{dy^2} + \dot{\gamma}z\frac{d\bar{\sigma}_{yz}}{dy} = 0 \tag{30}$$

The solution of Eq. (30) is

$$\bar{\sigma}_{yz}(\vec{r}) = A + b\exp\left(-\frac{\dot{\gamma}\varsigma yz}{kT}\right) \tag{31}$$

where A and b are constants.

Substituting Eq. (31) into equation (28) gives

$$\langle\sigma_{yz}\rangle_1 = A + \frac{b}{V_1}\int_{V_1}\left(1 - \frac{\dot{\gamma}\varsigma yz}{kT} + \cdots\right)d\vec{r} = \tag{32}$$
$$A + B\left(1 - \frac{2a^2\dot{\gamma}\varsigma}{5\pi} + \cdots\right) = A + B\exp\left(-\frac{2a^2\dot{\gamma}\varsigma}{5\pi}\right)$$

where A and B are constants.

Finally, substituting Eq. (31) into Eq. (27) it becomes

$$\eta(\dot{\gamma}) = \frac{A}{\dot{\gamma}} + \frac{B}{\dot{\gamma}}\exp\left[-C\frac{\dot{\gamma}}{kT}\eta(\dot{\gamma})\right] \tag{33}$$

where A, B and C are constants.

This equation is non linear. Taking $\eta\dot{\gamma} = X$, then Eq. (33) can be rewritten as

34

$$X = C + D\exp\left[-R\frac{X}{kT}\right]$$

For a fixed T, the solution of Eq. (34) is $\eta\dot{\gamma} = X$ = const., i.e.,

$$\eta(\dot{\gamma}) = \frac{\text{const}}{\dot{\gamma}} \tag{35}$$

Equation (35) shows that at meso-scale level viscosity is inversely proportional to the strain rate.

5. The viscosity at micro-scale level

Micro-level structure has the size of atoms or dislocations. At this level, there are point and linear defects. As mentioned in the Introduction section, it is necessary to distinguish deformation and fracture at micro-level under static loading condition and dynamic loading condition. Deformation and fracture process at micro-level under static loading are basically creep and diffusion, which factually takes place at the weakened boundaries between macro-structural elements. The creep and diffusion processes under static loading result in the separation of the body into macro-fragments. Therefore, the creep and diffusion under static loading are mainly concentrated at the weakened boundaries between macro-structural elements, and they may be attributed to the deformation proceeding at macro-structural level. At micro-level at high dynamic loading rate, deformation and fracture proceed uniformly at microscale level through the body without obvious localization of deformation and fracture. As a result of the high loading rate, the body is pulverized. The discussion in this section is focused on the deformation and fracture at micro-level under high dynamic loading rate.

Under intensive dynamic loading, viscosity of polycrystals is determined by the following equation [74]:

$$\eta = \frac{H}{\dot{\varepsilon}\ln\left(bN_m v_\infty/\dot{\varepsilon}\right)^2} \tag{36}$$

where v_∞ is the limit speed of dislocation; b is Burgers vector; N_m is the

density of movable dislocations; and H is a constant.

Equation (36) shows that when $\dot{\varepsilon} \to \infty$, $\eta \propto 1/\dot{\varepsilon}$. Therefore, at micro-scale levels viscosity is very small. Usually at this level viscosity is very low and varies in a range of 30–50 Pa s.

For polycrystalline rocks, for example rock salt, dislocation motion is the main mechanism of the deformation [68]. For non-crystalline rocks, at high strain rates because of the inertia effect rock samples are in confined triaxial stress state, microscopic slip bands prevail [41]; in this case, dislocation theory is applicable [52]. From the viewpoint of mechanism of deformation, fracture and energy dissipation in triaxial compression states rock mass behaves plastically. In addition to the a thermal growth of cracks, crack nuclei grow rapidly and uniformly throughout intact area due to the thermo-fluctuation deformation and breakage of the atomic bonds in the absence of significant stress concentration. The development of deformation and damage eventually results in the formation of microscopic slip bands. The presence of defects only results in the increase in the rate of deformation and breakages due to the local feature of energy dissipation in the deformation and fracture process of the materials. The last situation should cause the weak temperature dependence of the strength of materials in this condition. Therefore, from the viewpoint of deforming mechanism, fracture and energy dissipation the behaviors of metal polycrystals and rocks at very high strain rates are almost the same, and Eq. (36) is also valid for rock-like materials and is consistent with Eq. (35) for viscosity at meso-level.

6. Unified description of viscosity at different structural scale levels

Summarizing the analysis in Sects. 3, 4 and 5, we can see that viscosity at tectonic macro-level is very high and gradually decreases with the decrease in activated structural element size of rock mass. At meso-scopic and microscopic levels, viscosity is very low. In this section, we try to unify viscosity at different scale levels.

Equation (5) indicates that viscosity is determined by relaxation time. In turn, relaxation time is related to the effective relaxation speed. From the

phenomenological point of view, it can be assumed that the effective relaxation speed is a function of deformation rate and accelerates with the increase in strain rate:

$$\nu = \nu\left(\dot{\varepsilon}\right) \tag{37}$$

Expanding Eq. (37) into Taylor's series, it becomes

$$\nu\left(\dot{\varepsilon}\right) = \nu_0\left(0\right) + \alpha\dot{\varepsilon} + \cdots \tag{38}$$

where $v_0(0)$ may be regarded as growth speed of flaws at fixed magnitude of deformation.

For rock mass with the characteristic length L, assuming that relaxation time T is proportional to the propagation time of flaws, and when only a linear term is reserved in (38), relaxation time can be expressed as

$$T = \frac{L}{\nu_0 + \alpha\dot{\varepsilon}} \tag{39}$$

where α is a constant.

Although Eq. (39) is derived from a phenomenological point of view, its validity has been proved by in situ observations (Eq. 19). If the law of deformation and fracture of geological medium are similar to that of the Maxwell body, the reoccurrence period of earthquakes can be considered to be proportional to the relaxation time of rock mass. According to the statistics made by Sadovsky et al. [64], the reoccurrence period T of earthquakes and their energy have the relationship shown in Fig. 10:

$$\lg T\left(E\right) = 1/3\lg E - 3.5 \tag{40}$$

Fig. 10

Dependence of reoccurrence period of earthquakes on their energy (after Sadovsky et al. [64])

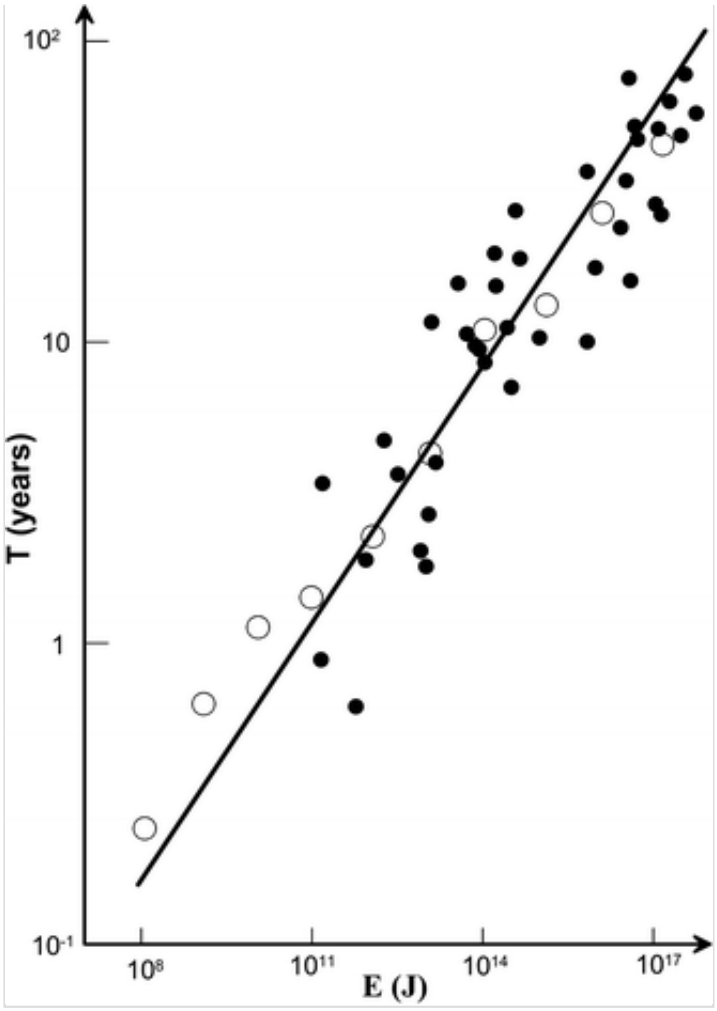

Considering that the energy of earthquakes is proportional to their source volume $V \sim L^3$, where L is the size of the earthquake source, Sadovsky and Pisarenko [63] suggested:

$$T \sim L \sim E^{1/3} \tag{41}$$

This relationship is valid for earthquakes with magnitudes 4–8.5.

It is interesting to note that according to the investigation by Kuksenko [35], the fracture time t_l is also proportional to the sample sizes ranging from the order of cm to that of km (Fig. 11).

Fig. 11

Influence of rock sample sizes on durability of their fracture (after Kuksenko [35])

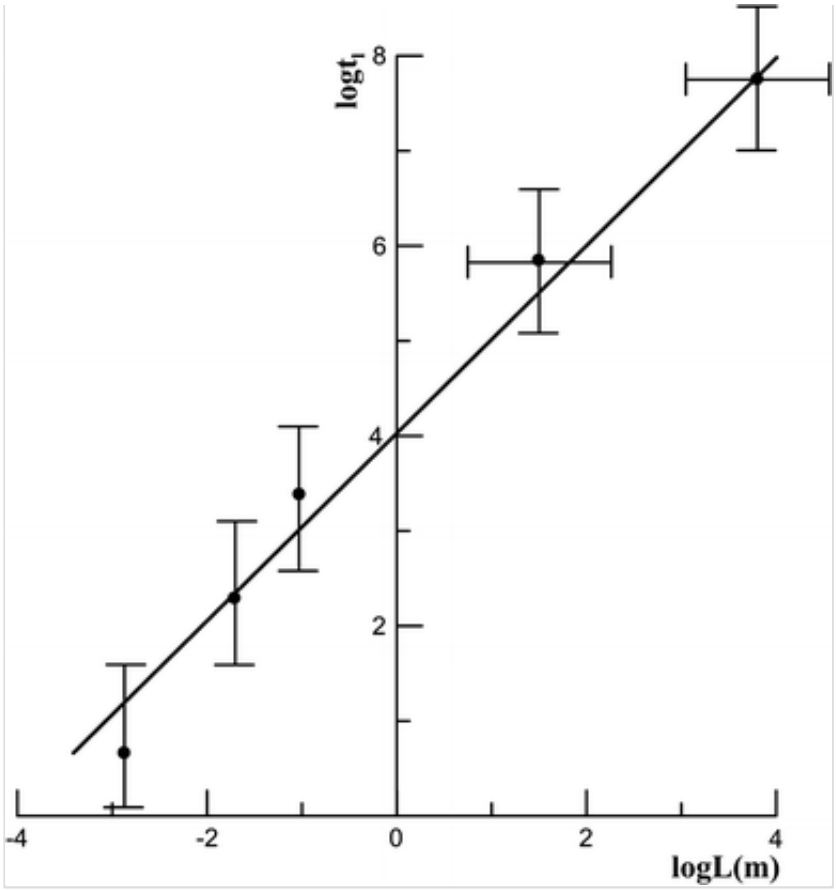

$$t_l \sim L \tag{42}$$

It reveals the intrinsic relationship between the structural scale levels and the relaxation time scale.

Therefore, the viscosity of materials can be expressed as

$$\eta = G \cdot \tau = G\alpha \frac{L}{\nu_0 + \alpha\dot{\varepsilon}} \tag{43}$$

In the case of a low deformation rate, this is consistent with Eq. (19). When $\dot{\varepsilon} \to \infty$, it is

$$\eta = G\alpha \frac{L}{\nu_0 + \alpha\dot{\varepsilon}} \propto \frac{1}{\dot{\varepsilon}} \tag{44}$$

which coincides with Eqs. (23) and (36).

Because of the diversity of materials, linear approximation of dependence of

growth speed v on strain rate is not sufficient to describe the complex behaviors of the media.

As demonstrated in Figs. 5 and 7, the dependence of crack growth speed on stress intensity factor and stress is nonlinear. This means that the dependence of growth speed of a crack on strain rate should be nonlinear. In the following, strain rate is taken as an independent variable.

As an approximation, considering the expression for the approximation of growth speed of crack in regimes II and III, we have

$$\nu = \nu_0 + b\left(\frac{\dot{\varepsilon}^n}{1+\lambda\dot{\varepsilon}^n}\right) \tag{45}$$

where b, λ and n are constants.

According to the Maxwell model under a given strain rate, the working scale level (activated scale level) is inversely proportional to the strain rate. Considering that when $\dot{\varepsilon} \to 0$ and the value of L is limited, taking

$$L \propto \frac{1}{\dot{\varepsilon}+d} \tag{46}$$

where d is a small constant.

Hence, viscosity can be expressed as

$$\eta = \frac{A}{\dot{\varepsilon}+d} + \frac{B+C\dot{\varepsilon}^n}{\nu_0+b_1\dot{\varepsilon}^n}\cdot\frac{1}{\dot{\varepsilon}+d} \tag{47}$$

where A, B, C, b_1 and n are constants.

At high and intermediate strain rates, considering that B and d are relatively small, Eq. (47) can then be rewritten as

$$\eta = \frac{A}{\dot{\varepsilon}} + \frac{C\dot{\varepsilon}^{n-1}}{\nu_0+b_1\dot{\varepsilon}^n} \tag{48}$$

It is clear from Eq. (48) that at low strain rates the first term in the right-hand

side of (48) plays a main role and the second term approximates to zero, whereas at high strain rates, it behaves another way around.

It is well known that at low strain rates, deformation and fracture are controlled by thermally activated mechanism, and at high strain rates, phonon (viscous) is the principal mechanism of deformation and fracture. Therefore, to clarify the physical meaning, Eq. (48) can be rewritten as follows

$$\eta = a_1 \frac{\ln(\dot{\varepsilon}/\dot{\varepsilon}_0)}{\dot{\varepsilon}} + a_2 \frac{(\dot{\varepsilon}/\dot{\varepsilon}_s)^{n-1}}{[(\dot{\varepsilon}/\dot{\varepsilon}_s)^n + 1]}, \quad n \geq 1 \tag{49}$$

where a_1 and a_2 are constants; $\dot{\varepsilon}_0$ is the strain rate of the order of 10^{12}/s, $\dot{\varepsilon}_s$ is a characteristic strain rate. As $\ln(\dot{\varepsilon}/\dot{\varepsilon}_0)$ varies slowly with strain rate $\dot{\varepsilon}$, Eqs. (48) and (49) coincide eventually. In this case, the first term on the right-hand side of Eq. (49) is in fact the contribution of the thermally activated mechanism of deformation, which can be seen from Eq. (53) in the following section, and the second term is the contribution of the macro-viscosity mechanism which can be expressed as,

$$\eta_{\text{mac}} = a_2 \frac{(\dot{\varepsilon}/\dot{\varepsilon}_s)^{n-1}}{[(\dot{\varepsilon}/\dot{\varepsilon}_s)^n + 1]} \tag{50}$$

7. Application of the unified model to description of strain rate sensitivity of rock

The general feature of strength–strain rate dependence of brittle materials is illustrated in Fig. 12 [23, 26]. In the lower strain rate range identified as regime I, the material strength increases slowly with the increase in strain rate. In the intermediate strain rate range in regime II, the strain rate sensitivity is characterized by a rapid strength increase when the strain rate exceeds a threshold. At very high strain rate in regime III, the strength dependence becomes weak again, similar to that in regime I.

Fig. 12

Dependence of dynamical strength on strain rates of brittle materials ($\dot{\varepsilon}_1 \approx 10^0$–$10^2$ s^{-1}, $\dot{\varepsilon}_s \approx 10^2$ to 10^3 s^{-1}; $\dot{\varepsilon}_2 \approx 10^4$ to 10^5 s^{-1}) (after Grady, Hollebach et al. [23, 26])

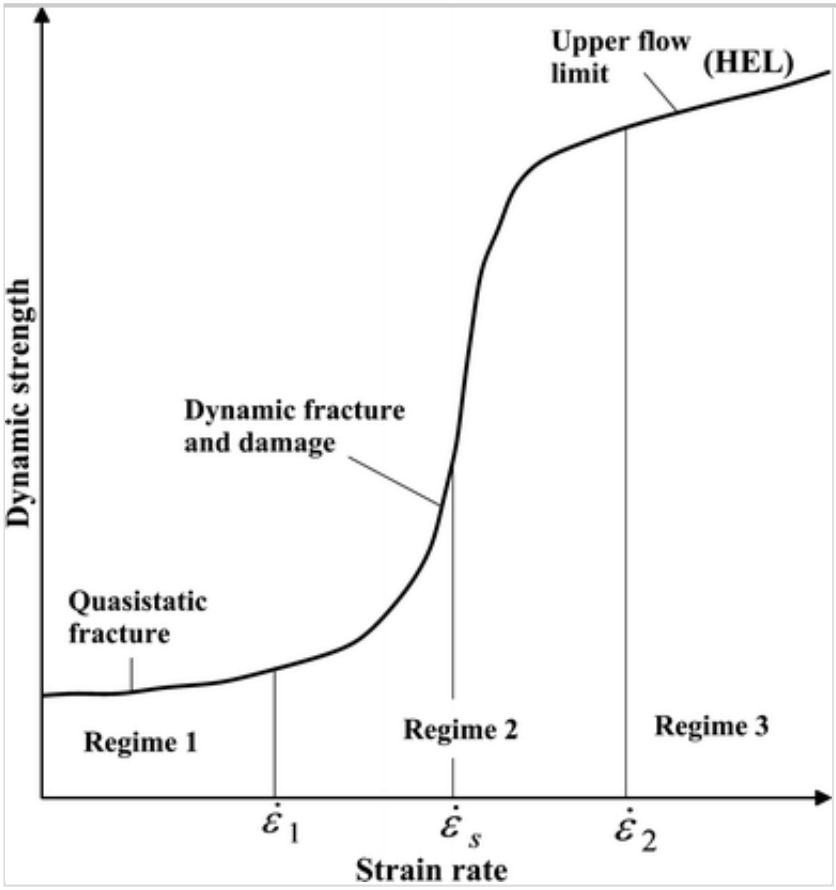

Under moderate uniaxial tension ($\sigma_z < \sigma < U_0/U_0\gamma.\gamma$, where σ_z is determined by $\Delta F(\sigma_z) = kT$, with $\Delta F(\sigma_z)$ denoting the decrease in free energy due to the action of external stress), this situation corresponds to regime I in Fig. 11. The expected lifetime (loading time to failure) τ may be determined by the formula [80]

$$\tau = \tau_0 \exp\left(\frac{U_0 - \gamma\sigma}{kT}\right) \tag{51}$$

where U_0 is the activation energy; σ is the uniaxial tensile stress; γ is the activation volume; k is the Boltzmann constant; T is absolute temperature; τ_0 is a temporal parameter in the order of Debye's vibration period of atoms (about 10^{-12} s).

Zhurkov's formula indicates the thermo-activated nature of deformation and fracture. From it, we can obtain the dependence of the strength Y_T on the lifetime τ (loading time to failure)

$$\sigma = Y_T = \frac{1}{\gamma}\left(U_0 + kT\ln\frac{\tau_0}{\tau}\right) \tag{52}$$

If we express the lifetime τ as $\tau = \varepsilon_0/\dot{\varepsilon}$, where ε_0 is the limit of deformation at failure, and $\dot{\varepsilon}$ is the characteristic strain rate of loading process; from Eq. (53), we have

$$Y_T = \frac{1}{\gamma}\left(U_0 + kT\ln\frac{\dot{\varepsilon}}{\dot{\varepsilon}_0}\right) \tag{53}$$

where $\dot{\varepsilon}_0 = \varepsilon_0/\tau_0$ represents the maximum possible strain rate in material.

Equation (53) indicates the thermal activation nature of strength of materials and describes adequately the strain rate sensitivity in regime I.

Regimes II and III are dynamic loading regimes. The distinctive feature of any dynamic loading process in comparison with the static one is the appearance of inertial effect in dynamic loading process, which induces overloading (strength enhancement) in a solid material. But the final level of overloading is eventually determined by the proceeding in solid material kinetic fracture process (stress relaxation process), i.e., by the time from the beginning of loading to the moment of failure, which can be characterized by viscosity. The smooth transition from regime I to regime II represents a gradual change, i.e., the thermo-activated mechanism gradually loses its predominance and viscosity gradually emerges as the dominant mechanism [50]. However, these two mechanisms coexist. At very high strain rates, because of the finiteness of crack propagation speed a wide range of crack sizes is simultaneously initiated in the material [32]. In intact areas, the thermo-activated mechanism is initiated again, and the atomic bonds are broken. These broken bonds will further serve as the growing athermal nuclei of damage. This implies that the localization of the deformation and damage is gradually lost. Thus, the thermo-activated mechanism again emerges as the dominant mechanism of the deformation and fracture at high strain rates [53, 54]. Equation (53) is therefore also applicable for the case of high strain rate.

From the viewpoint of structural hierarchy at low strain rates, deformation

and fracture take place at the weakened boundaries between macro-structural elements. Therefore, they may be attributed to the deformation proceeding at macro-structural levels. The result of deformation and fracture at slow strain rates is the separation of the body into macro-fragments. With the increase in strain rates, according to Eq. (11) meso-scale and micro-scale levels of rock mass are successively involved in deformation and fracture processes, and the fragment size decreases successively. At very high strain rates, deformation and fracture proceed at micro-scale level uniformly, and the material is pulverized. Therefore, for samples of definite size, with the increase in strain rate macro-scale, meso-scale and micro-scale levels will be involved in deformation and fracture processes, i.e., the scale level at which deformation and fracture proceed decreases gradually, and the viscosity model developed in the previous sections may be used for modeling of viscous contribution to dynamic strength of rock mass with the increase in strain rate.

Therefore, in regime II Eq. (53) should consider the contribution of macro-viscosity $Y_{\text{macv}} = \eta_{\text{mac}}\dot{\varepsilon}$:

$$Y = Y_T(\dot{\varepsilon}) + Y_{\text{macv}}(\dot{\varepsilon}) = \frac{1}{\gamma}\left(U_0 + kT\ln\frac{\dot{\varepsilon}}{\dot{\varepsilon}_0}\right) + a_2\frac{(\dot{\varepsilon}/\dot{\varepsilon}_s)^n}{[(\dot{\varepsilon}/\dot{\varepsilon}_s)^n + 1]} \tag{54}$$

To verify the effectiveness of the given model, some calculations are performed using Eq. (54), and the results are compared with experimental data by Grady [26]. Being almost horizontal straight lines, the left parts of the curves in Fig. 12 represent the contribution of thermo-activation. These lines are chosen as the basis for superposing the contribution of macro-viscosity; hence, the first term on the right-hand side of Eq. (54) is not needed, and only the second term is used. The experimental curves for granodiorite and dolomite are approximated with the parameters shown in Fig. 13. It is clear from the curves that the approximation is adequate. This indicates that Eq. (50) has a sound physical basis. It is applicable to a wide range of strain rates and is simple and convenient for practical use.

Fig. 13

Comparison of calculation with the experimental data (*triangle* and *square* are experimental curves (after Drady et al. [41]); *cross* are approximation curves).

Values of parameters: curve 1 (granodiorite): $b = 4.3$, $\dot{\varepsilon}_s = 10^{1.7}$, $n = 1.5$; curve 2 (dolomite): $b = 2.0$, $\dot{\varepsilon}_s = 10^{2.8}$, $n = 1.0$

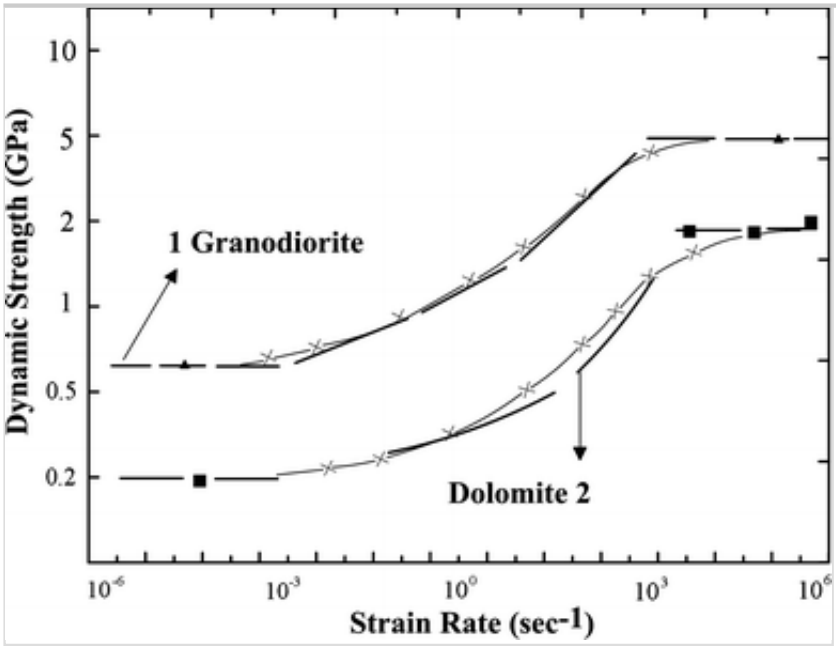

8. Conclusions

Based on available data on relationship between viscosity and structural hierarchy of rock mass, rheological properties of rock mass at different structural levels are examined. The following conclusions can be drawn:

1. Viscosity and characteristic strain rate are different at different structural levels. At the macroscopic level, the characteristic strain rate is low with high viscosity, whereas at micro- to meso-levels the characteristic deformation rate is high and viscosity is low.

2. With the increase in external loads and strain rate, the deformation and fracture consecutively cover meso-scopic to microscopic levels, and viscosity decreases gradually. At high strain rate, viscosity is inversely proportional to strain rate. Hence, viscosity is not a constant of materials, but depends on the structural level at which deformation and fracture take place.

3. Based on the analysis, a unified description of viscosity at different structural levels is proposed. The unified descriptions of viscosity in limit cases are valid for continental and micro-scale levels. This

suggests that the unified description is adequate for the description of viscosity at different structural levels of rock mass.

4. The application of unified description for viscosity to description of the strength–strain rate sensitivity of rocks shows the effectiveness of the obtained result.

Acknowledgments

The study was financially supported in part by the National Natural Science Foundation of China (Nos. 51174012 and 51478027), the Project of Construction of Innovative Teams and Teacher Career Development for Universities and Colleges Under Beijing Municipality (No. IDHT20130512), the “973” Key State Research Program (Grant No. 2015CB0578005), Science Fund for Creative Research Groups of the National Natural Science Foundation of China (No. 51021001), as well as Development of High-Caliber Talents Project of Beijing Municipal Institutions granted to Dr. Jilin Qi (No. CIT&TCD20150101).

References

1. Anderson O, Grew P (1977) Stress corrosion theory of crack propagation with application to geophysics. Rev Geophys Space Phys 15:77–104

2. Ando R, Yamashita T (2007) Effects of mesoscopic-scale fault structure on earthquake ruptures: dynamic formation of geometrical complexity of earthquake faults. J Geophys Res 112:B09303. doi:10.1029/2006JB004612

3. Altshuler LV, Doronin GS, Kim GKh (1987) Viscosity of shock compressed liquids. App Mech Tech Phys 28(6):110–118

4. Atkinson B (1984) Subcritical crack growth in geological materials. J Geophys Res 89:4077–4114

5. Atkinson B, Meredith P (1987) The theory of subcritical crack growth

with application to minerals and rocks. In: Fracture mechanics of rock. Academy Press, New York, pp 111–166
AQ2

6. Barton CC (1995) Fractal analysis of scaling and spatial clustering of fractures. In: Barton CC, Lapointe PR (eds) Fractal in the earth science. Plenum Press, New York, pp 141–178

7. Belinsky IV, Khristoforov BD (1968) Viscosity of NaCl under shock compression. Appl Mech Tech Phys 9(1):150–151

8. Belinsky IV, Mikhaliuk AV, Khristoforov BD (1975) Viscosity of rock mass in deformation processes. Phys Solid Earth 11(8):80–84

9. Bieniawski ZT (1967) Mechanism of brittle fracture of rock: part I theory of fracture process. Int J Rock Mech Min Sci Geomech Abstr 4(4):395–406

10. Bird RB, Armstrong RC and Hassager O (1987) Dynamics of polymeric liquid, vol. 2, 2-nd ed. Wiley, New York

11. Broberg KB (1999) Cracks and Fracture. Academic Press, San Diego

12. CEB (1993) CEB-FIP model code 1990. Committee Euro-International Du Beton, Redwood Books, Trowbridge, Wiltshire

13. Chekunaev NI, Kaplan AM (2009) Limiting speed of crack propagation in elastic materials. J Appl Mech Tech Phys 50(4):677–683

14. Chow TS (2000) Mesoscopic physics of complex materials. Springer, New York

15. Dove PM (1995) Geochemical controls on the kinetics of quartz fracture at subcritical tensile stresses. J Geophys Res 100:22349–22359

16. Dulaney EN, Brace WF (1960) Speed behavior of a growing crack. J Appl Phys 31(12):2233–2236

17. Faulkner D, Jackson CAL, Lunn RJ, Schlische RW, Shiptone ZK, Wibberley CAJ, Withjack MO (2010) A review of recent developments concerning the structure, mechanics and fluid flow properties of fault zones. J Struct Geol 32(11):1557–1575

18. Field JE (1971) Brittle fracture: its study and application. Comtemp Phys 12(1):1–31

19. Fineberg J, Marder M (1999) Instability in dynamic fracture. Phys Rep 313:101–108

20. Finkel VM (1962) Investigation on crack growth under dynamic fracture of glass. Phys Solid State 4(6):1412–1418

21. Freiman S (1984) Effects of chemical environments on slow crack growth in glasses and ceramics. J Geophys Res 89:4072–4076

22. Freund LB (1990) Dynamic fracture mechanics. Cambridge University Press, Cambridge

23. Grady DE (1996) Shock wave properties of brittle solids. In: Schmidt Steve (ed) Shock compression of condensed matters, 9–20. AIP Press, New York

24. Grady DE (2008) Fragment size distribution from the dynamic fragmentation of brittle solids. Int J Impact Eng 35(12):1557–1562

25. Grady DE (2010) Length scale and size distribution in dynamic fragmentation. Int J Fract 63:85–99

26. Grady DE, Hollebach RE, Schuler KW, Callender JF (1977) Strain rate dependence in Dolomite inferred from impact and static compression rests. J Geophs Res 82:1325–1333

27. Hadley K (1976) Comparison of computed and observed crack densities and seismic velocities in Westerly granite. J Geophys Res 81:3484–3494

28. Hong L, Li XB, Ma C, Yin TB, Ye ZY, Liao GY (2008) Study on size effect of rock dynamic strength and strain rate sensitivity. Chin J Rock Mech Eng 27(3):526–533

29. Horie Y, Yano K (2002) Non-equilibrium fluctuations in shock compression of polycrystalline α-iron. In: Furnish MD (ed) Shock compression of condensed matter-2001. AIP, New York, pp 553–556

30. Housen KR, Holsapple KA (1999) Scale effects in strength-dominated collisions of rocky asteroids. Icarus 142:21–33

31. Kipp ME, Grady DE (1985) Dynamic fracture growth and interaction in one dimension. J Mech Phys Solids 33(4):399–415

32. Kipp ME, Grady DE, Chen EP (1980) Strain-rate dependent fracture initiation. Int J Fract 16:471–478

33. Kocharyan GG (2014) Scale effect in seismotectonics. Geodyn Tectonophys 5(2):353–385. doi:10.5800/GT2014520133

34. Kocharyan GG, Kulyukin AA, Markov VK, Markov DV, Pavlov DV (2005) Small disturbances and stress-strain state of the Earth's crust. Phys Mesomech 8(1):23–36

35. Kuksenko VS (1987) Physical and methodological fundament for prediction of rock-bursts. J Min Sci 23(1):9–22

36. Kurlenia MV, Oparin VN (1996) Scale factor of phenomenon of zonal disintegration of rock and canonical series of atomic and ionic radii. J Min Sci 32(2):81–90

37. Kurlenia MV, Oparin VN, Eremenko AA (1993) Relation of linear block dimensions of rock to crack opening in the structural hierarchy of masses. J Min Sci 29(3):197–203

38. Landau LD, Lifshitz EM (1959) Theory of elasticity. Pergamon, London

39. Lawn BR, Wilshaw TR (1975) Fracture of brittle solids. Cambridge University Press, Cambridge

40. Lee J (2002) The universal role of turbulence in the propagation of strong shocks and detonation waves. In: Horie Y (ed) High-pressure shock and compression of solids VI. Springer, Berlin, pp 121–148

41. Lindholm US, Yeakley LM, Nagy A (1974) The dynamic strength and fracture properties of Dresser basalt. Int J Rock Mech Min Sci Geomech Abstr 11(5):181–191. doi:10.1016/0148-9062(74)90885-7

42. Lockner DA, Moore RM, Reches Z (1992) Microcrack interaction leading to shear failure. In: Tillerson JR, Wawersik WR (eds) Rock Mechanics, Proceedings of the 33rd US Symposium. Balkema, The Netherland, pp 807–817

43. Lysak SV, Levi KG (1992) Continental rift zone patterns and their geophysical fields. In: Logatchev NA (ed) Faulting in lithosphere, extensional zones. Nauka, Siberian Branch, Novosibirsk, pp 6–21

44. Moore RM, Lockner DA (1995) The role of microcracking in shear fracture propagation in granite. J Struct Geol 17:95–114

45. Mott NF (1948) Brittle fracture in mild steel plates. Engineering 165:16–18

46. Oparin VN, Yushkin VF, Akinin AA, Balmashnov EG (1998) A new scale of hierarchically structured representations as a characteristic for ranking entities in a geomedium. J Min Sci 34(5):387–401

47. Ožbolt J, Rah KK, Mestrović D (2006) Influence of loading rate on concrete cone failure. Int J Frac 139:239–252

48. Panin VE (1998) Physical mesomechanics of heterogeneous media and computer-aided design of materials. Cambridge Int Sci Pub, Cambridge

49. Petrov VA (1984) Lifetime of solids under low loads-nonfracturing stresses. Phys Solid State 26(7):2116–2119

50. Perzyna P (1998) Constitutive modeling of dissipative solid for localization and fracture. localization and fracture phenomena in inelastic solids. Springer, Wien, New York, pp 99–241

51. Piggot AR (1997) Fractal relations for the diameter and trace length of disc-shaped fractures. J Geophys Res 102:18121–18125

52. Popov VL, Kröner E (2001) Theory of elastoplastic media with mesostructure. Theo App Fra Mech 37(1–3):299–310

53. Qi CZ, Qian QH (2003) Physical mechanism of brittle material strength-strain rate sensitivity. Chin J Rock Mech Eng 21(2):177–181

54. Qi CZ, Qian QH (2009) Basic problems of dynamic deformation and fracture of rock mass. Science Press, Beijing

55. Qi CZ, Wang MY, Bai JP, Li KR (2014) Mechanism underlying dynamic size effect on rock mass strength. Int J Impact Eng 68:1–7

56. Chengzhi Qi, Mingyang Wang, Qihu Qian, Jianjie Chen (2008) Structural hierarchy of rock masses and the mechanisms of its formation. Moscow University Mech Bull 63(5):113–121. doi:10.3103/S0027133008050026

57. Radionov VN, Sizov IA, Tsvetkov VM (1986) Fundamental of geomechanics. Nedra, Moscow

58. Rahiman TIH, Pettinga JR (2009) Fracture lineaments, fault mesh formation and seismicity: towards a seismotectonic model for Viti Levu, Fiji. Bull New Zealand Soc Earth Eng 42(1):63–72

59. Roberts DK, Wells AA (1954) The speed of brittle fracture. Engineering 24:820–821

60. Rosakis AJ, Samudrala O, Coker D (1999) Cracks faster than the shear wave speed. Science 284:1337–1340

61. Rouleau A, Gale JE (1985) Statistical characterization of the fracture system in the Stripa granite. Int J Rock Mech Min Sci Geomech Abstr 22:353–367

62. Sadovsky MA, Bolkhovitinov LG, Pisarenko VF (1987) Deformation of geophysical medium and seismic process. Publishing house “Nauka”, Moscow (In Russian)

63. Sadovsky MA, Pisarenko VF (1983) On dependence of preparation time of earthquake on its energy. Rep Acad Sci USSR 271(2):330–333

64. Sadovsky MA, Pisarenko VF, Shteinberg VV (1983) On dependence of energy of earthquake on earthquake source volume. Rep Acad Sci USSR 271(3):598–602

65. Salganik R, Rapoport L, Gotlib VA (1997) Effect of structure on environmentally assisted subcritical crack growth in brittle materials. Int J Fract 87:21–46

66. Savage HM, Brodsky EE (2011) Collateral damage: Evolution with displacement of fracture distribution and secondary fault strands in fault damage zones. J Geophys Res 116(B3):B03405

67. Scholz CH, Dawers NH, Yu JZ, Anders MH, Cowie PA (1993) Fault growth and scaling laws: preliminary results. J Geophys Res 98:21951–21961

68. Senseny PE, Hansen FD, Russell JE, Carter NL, Hardin JW (1992) Mechanical behavior of rock salt: Phenomenology and micro-mechanism. Int J Rock Mech Min Sci Geomech Abstr 29(4):363–378

69. Sherman SI (1992) The relationships between quantitative parameters of faults. In: Logatchev NA (ed) Faulting in lithosphere, extensional zones. Nauka, Siberian Branch, Novosibirsk, pp 78–102

70. Sherman SI (2012) Destruction of the lithosphere: fault-block divisibility and its tectonophysical regularities. Geophys Tectonophys 3(4):315–344

71. Shibi T, Kamei T (2008) Investigation of the mechanism of fault formation using bifurcation analysis. In: Proceedings of the eighteenth international offshore and polar engineering conference, 654–659. Vancouver, BC, Canada, July 6–11

72. Sih GC (2008) Birth of mesomechanics arising from segmentation and multiscaling: nano-micro-macro. Phys Mesomech 11(3–4):128–140

73. Spahn F, Neto EV, Guimaraes AHF, Gorban AN, Brilliantov NV (2011) A statistical model of aggregates fragmentation. Eprint arXiv: 1106.2721lvl [cond-mat-stat-mech] 14 Jun 2011

74. Stepanov GV, Kharchenko VV (1984) Relation between stress and strain in metals under impulsive action. Probl Strength 11:32–37

75. Steverding B, Lehnigk SH (1970) Response of cracks to impact. J Appl Phys 41(5):2096–2099

76. Tyapkin KF, Kiveliuk TT (1982) Investigation of fault structure by geological-geophysical methods. Nedra, Moscow

77. Wang TM (2006) Control of cracking in engineering structures. China Architecture & Building Press, Beijing

78. Yavari A, Khezrzadeh H (2010) Estimating terminal speed of rough cracks in the framework of discrete fractal fracture mechanics. Eng Fra Mech 77(10):1516–1526

79. Yoffe EH (1951) The moving Griffith crack. Phil Mag 42:739–750

80. Zhurkov SN (1965) Kinetic concept of the strength of solids. Int J Fract 1(4):311–322